Film Deposition Methods

1 Introduction

The deposition of thin-film functional layers on different substrates is an essential step in many fields of modern high technology, and applications range from large-area optical coatings on architectural structures to tribological layers, high-temperature superconductors, and finally to applications in micro- and nanoelectronics. Considering this broad spectrum of applications it is obvious that there cannot be one perfect deposition method which can be applied in all fields. In contrast, there is a wide spectrum of methods all on a high level of development and it is sometimes difficult to make the optimum choice. Even within the special field of information technology films of very different materials have to be considered: semiconductors, metals, especially magnetic layers, dielectric and ferroelectric oxides and organic layers. The deposition methods are dominated by depositions from the vapour phase and we will concentrate on the basic principles of these methods. A selection of vapour deposition methods is summarized in Table 1 with the generally accepted subdivision into physical and chemical methods. Physical methods may be characterized by a locally well-defined particle source and generally a free flight in vacuum to the substrate. For chemical methods, the so-called precursor molecules fill the reactor vessel as a vapour, dissociate at the hot substrate surface and release the atoms of interest. Some basic characteristics of the methods are summarized, however, the characterization is sometimes not very specific as the parameters depend strongly on the properties of the material of actual interest. Hence, there are many such comparisons in the literature showing some dependence on the personal bias of the author. A short introduction to depositions from solution is included in Sec. 4: i.e. chemical solution deposition (CSD) and the Langmuir-Blodgett method for monomolecular organic films. Of course, the list is not complete and we must refer to the literature for additional methods like electroplating (galvanic deposition) or thermal spray techniques.

	Physical Vapor Deposition			**Chemical Vapor Deposition**
	Evaporation / MBE	**Sputtering**	**PLD**	**CVD / MOCVD**
Mechanism of production of depositing species	Thermal energy	Momentum transfer	Thermal energy	Chemical reaction
Deposition rate	High, up to 750,000 Å/min	Low, except for pure metals	Moderate	Moderate Up to 2,500 Å/min
Deposition species	Atoms and ions	Atoms and ions	Atoms, ions and clusters	precursor molecules dissociate into atoms
Energy of deposited species	Low 0.1 to 0.5 eV	Can be high 1-100 eV	Low to high	Low; Can be high with plasma-aid
Throwing power a) Complex shaped object	Poor, line of sight	Nonuniform thickness	Poor	Good
b) Into blind hole	Poor	Poor	Poor	Limited
Scalable to wafer size	up to large	up to large	limited	up to large

Table 1: Some Characteristics of Vapour Deposition Processes (modified after Bunshah [1]).

2 Fundamentals of Film Deposition

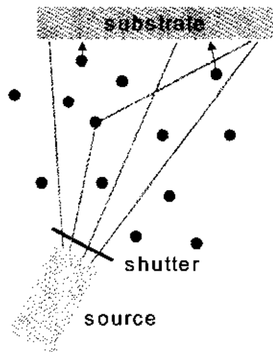

Figure 1: Schematics of a deposition system.

In this section, we introduce some fundamentals of film deposition which are valid for all methods. We start with the kinetics of gases as the residual gas pressure in the system determines the free path length of the deposited species and the possible incorporation of foreign atoms. Next, we discuss some basic thermodynamic data, like **vapour pressure** and **phase diagrams**, and their dependence on the residual gas pressure. Finally, we introduce the basic models for the nucleation and growth of thin films and the accommodation and release of lattice strain.

2.1 Gas Kinetics

The residual gas pressure in the system is one of the basic parameters to be controlled during film deposition as the residual gas atoms may collide with the depositing species or may hit the growing surfaces and may thus be incorporated in the film, Figure 1. For the simplest assumption that the gas atoms may be considered as not interacting masses with a Maxwell velocity distribution we obtain the mean free path length, λ, of the atoms or molecules

$$\lambda = \frac{1}{\sqrt{2}\pi N d^2} \tag{1}$$

d = molecular diameter, N = concentration of the gas. With the law of the ideal gas: $N = p/k_B T$, k_B = Boltzmann constant, we obtain:

$$\lambda = \frac{k_B T}{\sqrt{2}\pi p d^2} \tag{2}$$

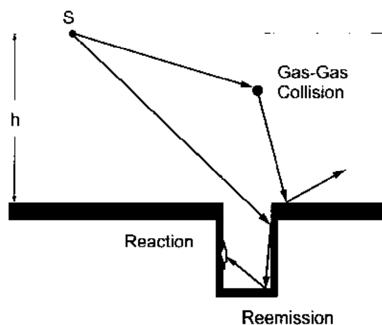

Figure 2: Deposition into a hole (after ref. 20). The example of an atom with starting position, S, with a height, h, above the substrate illustrates that either gas-gas collisions or reflection from the surface are necessary for a uniform deposition on bottom and sidewalls of a hole.

For the example of air molecules we obtain a free path length which is of the order of a typical distance from source to substrate of about 20 cm at a pressure of $0.5 \cdot 10^{-3}$ mbar. This rather moderate vacuum level shows that the beam interaction is not a critical condition for the base vacuum. More critical is the number of residual gas atoms which hit the growing surface and limit the purity of the film if they are incorporated. This number can be expressed as

$$N_i = p_i \sqrt{\frac{1}{2\pi k_B m_i T}} \tag{3}$$

m_i = atomic or molecular mass. Typical results are summarized in Tab. 2. Assuming a sticking coefficient of unity, the incorporation of residual gas atoms may be expressed in terms of monolayers and this growth rate may be rather high as compared to a typical growth rate of an epitaxial film i.e., one monolayer / s. Hence, for clean films **ultra-high vacuum** (UHV, better than 10^{-9} mbar) may be necessary.

A further aspect where the mean free path of the molecules becomes important is deposition into very small structures like small via or trenches, as they are becoming more and more important with increasing miniaturization of ICs, Figure 2. Comparing the dimensions of such submicron structures with the free path lengths of Table 2 we see that even for medium vacuum conditions the mean free path of the molecules becomes much larger than the structure size. Hence, for these conditions there is no gas collision within the holes, and for the distribution of the atoms reflection at the surfaces becomes important. For simulations of the deposition processes continuum gas dynamics must be supplemented by Monte Carlo methods.

p, mbar	**Mean free path, cm** (between collisions)	**Collisions / s** (between molecules)	**Molecules/(cm² s)** (sticking surface)	**Monolayer / s***
10^0	$6.8 \cdot 10^{-3}$	$6.7 \cdot 10^6$	$2.8 \cdot 10^{20}$	$3.3 \cdot 10^5$
10^{-3}	$6.8 \cdot 10^0$	$6.7 \cdot 10^3$	$2.8 \cdot 10^{17}$	$3.3 \cdot 10^2$
10^{-6}	$6.8 \cdot 10^3$	$6.7 \cdot 10^0$	$2.8 \cdot 10^{14}$	$3.3 \cdot 10^{-1}$
10^{-9}	$6.8 \cdot 10^6$	$6.7 \cdot 10^{-3}$	$2.8 \cdot 10^{11}$	$3.3 \cdot 10^{-4}$

* Assuming the condensation coefficient is unity

Table 2: Some facts about residual air at 25 °C in a typical vacuum used for film deposition (after Chopra [2]).

2.2 Thermodynamics

Phase-diagrams are the starting point for considering the deposition of a new material in order to see the stability range of the envisaged phase and the existence of concurrent phases. Standard phase diagrams are given at ambient pressure, however, changes with pressure must be considered for vacuum deposition methods. Figure 3 shows as a simple example the phase diagram of the completely intermixing binary system Si-Ge and the change from ambient pressure down to the UHV region [3]. At 1 mbar there is not much change compared to atmospheric pressure and we **observe** a wide range of stability of the mixed homogeneous crystalline phase, c, of Si-Ge (the decomposition of this homogeneous phase into two crystalline phases of different stoichiometry, c'and c'', at very low temperature is somewhat speculative). At higher temperatures the liquid, l, to solid (crystalline) phase transition is indicated and above 2000 K the liquid to vapour, v, transition is shown. With decreasing pressure there is a strong decrease in temperature of the l-v borderlines and even an overlap with the c-l lines. Finally, in the UHV region, 10^{-9} mbar, the liquid has disappeared and only direct sublimation, c→v, is left at temperatures around 1100 K. Hence, re-evaporation of the material under UHV conditions and high temperatures must be considered. In addition, a comparison with the deposition rates and gas pressures discussed along with Table 2 shows that the deposition of the films usually proceeds under high supersaturation, i. e. conditions far from thermodynamic equilibrium.

Vapour pressures and the related evaporation rates present another field of basic thermodynamic data, which are very useful for the control of the deposition of different compounds. Such data can be deduced from thermodynamic data tables (e.g., CODATA and JANAF) [4]. As an illustrative example we consider Pb-based perovskite oxides (such as $Pb(Zr,Ti)O_3$, PZT for short) which are the most important class of ferroelectrics for thin film applications. The deposition of these lead-based oxides is complicated by the fact that PbO is known as a very volatile oxide. Figure 4 shows the evaporation of PbO under atmospheric conditions and under UHV: under atmospheric pressure the volatile species is PbO and the vapour pressure of Pb is 3 orders of magnitude lower. In contrast, under UHV conditions the dominant species in the vapour phase is Pb.

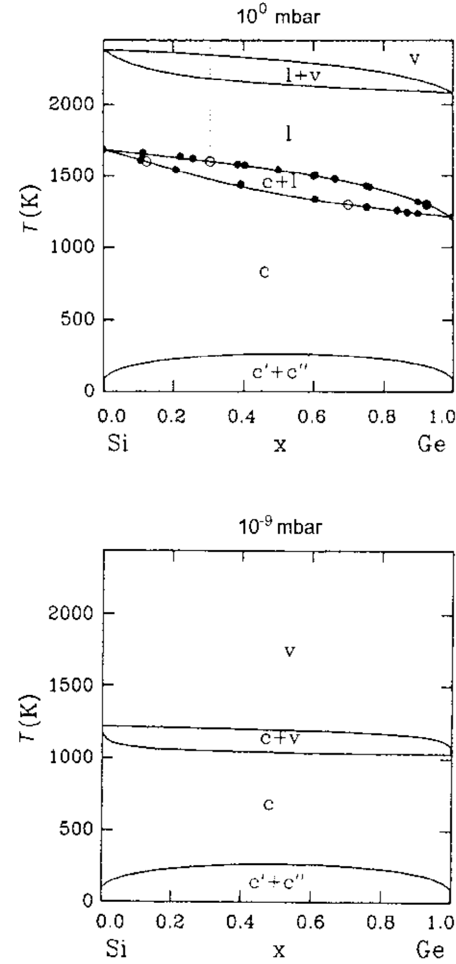

Figure 3: x–T phase diagram of the $Si_{(1-x)}$-Ge_x systems at 10^0 and 10^{-9} mbar [3]

2.3 Film Growth Modes

Nucleation and growth of a film proceeds from energetically favourable places on a substrate surface and even the cleanest polished surface shows some structure. Figure 5 shows schematically the structure of a well-polished single-crystal surface. The charac-

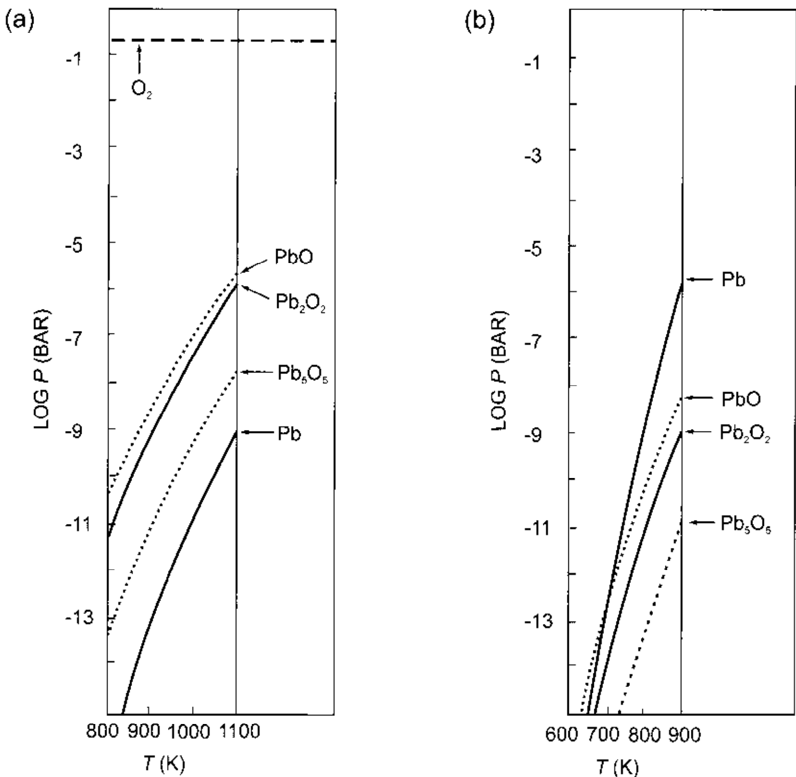

Figure 4: Vaporization of PbO at different oxygen partial pressures, (a) 0.2 bar and (b) 10^{-15} bar [4].

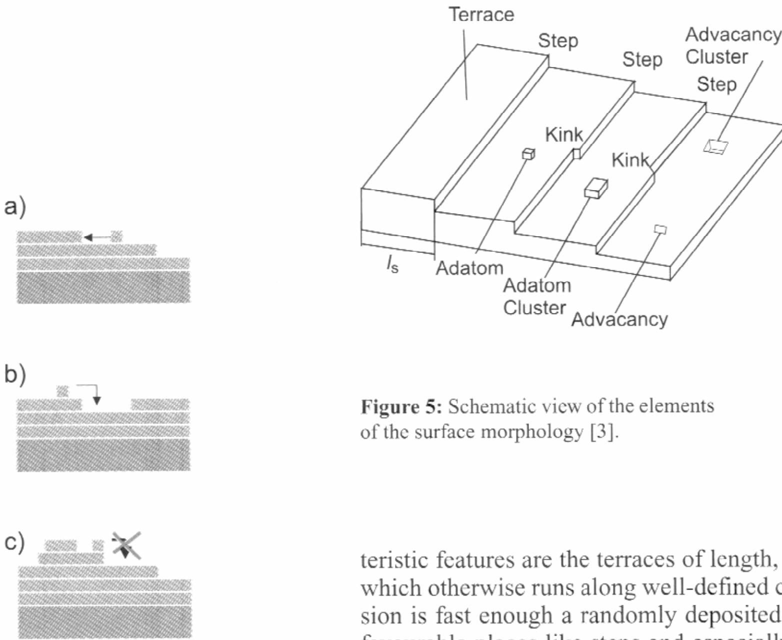

Figure 5: Schematic view of the elements of the surface morphology [3].

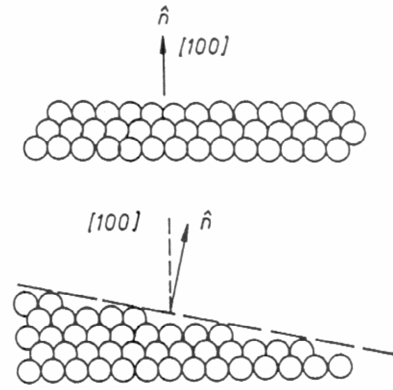

Figure 6: Change of the step distance, l_s, by cutting a surface at a small angle to a major crystallographic direction, i.e., forming a vicinal surface.

a)

b)

c)

Figure 7: Growth modes of homoepitaxy:
(a) step-propagation,
(b) 2d-island growth, and
(c) multi-layer growth.

teristic features are the terraces of length, l_s, the steps and the kinks within the step line, which otherwise runs along well-defined crystallographic directions. If the surface diffusion is fast enough a randomly deposited adatom will diffuse to the energetically most favourable places like steps and especially kinks. If at lower temperatures the diffusion is slower, several mobile adatoms may encounter each other within a terrace and may form additional immobile adatom clusters within the terraces. Similarly, advacancies and their clusters might be formed at the end of the coverage of a terrace. By reducing the step distance and hence the diffusion length by vicinal surfaces, Figure 6, the step controlled growth may be extended to lower temperatures,.

The details of the growth modes for the simplest case of **homoepitaxy**, the growth of a film on a single-crystalline surface of the same material, is indicated in Figure 7. As discussed above, step propagation dominates at higher temperatures and/or small deposition rates and two-dimensional island growth will predominate if immobile clusters are formed by the encounters of mobile adatoms. This simple picture is, however, quite frequently modified: if the jump across the step is kinetically hindered multilayer growth will be observed. This enlarged activation energy for the jump across the step is called the Ehrlich-Schwoebel effect and can be understood in a simple model as the adatom is nearly dissociated from the surface in the saddle point of this jump.

If we want to grow an epitaxial film on a different substrate (so-called **heteroepitaxy**), two material parameters have to be considered in addition: the surface energy, γ, and the lattice parameter or lattice match of the two materials. For the case of good lattice match the difference in surface energy leads to two different growth modes as indicated in Figure 8a and b. As long as :

$$\gamma_{\text{layer}} + \gamma_{\text{substrate/layer}} \leq \gamma_{\text{substrate}} \tag{4}$$

we observe perfect wetting and pure layer by layer or *Frank-van-der-Merve growth*. For the opposite case, we observe island or *Volmer-Weber growth*. For this consideration the surface energies of the crystallographic orientations of actual interest must be applied, which are often not available in data reference tables. If there is a lattice mismatch between substrate and film, an additional growth mode may be observed as indicated in Figure 8c, *Stranski-Krastanov growth*. A first layer may grow matched to the substrate, which yields additional strain energy. With growing thickness this strain energy increases in proportion to the strained volume and an island formation may become more favourable in spite of the larger surface area.

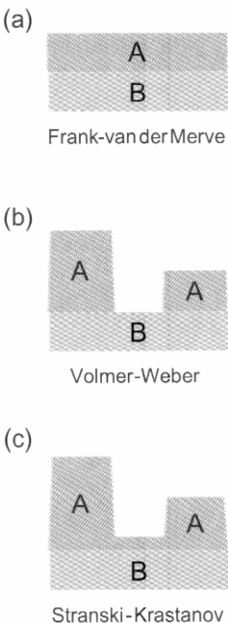

Figure 8: Growth modes of the hetero-epitaxy.

The contributions of strain and surface energy can quite generally be described in a simple model and the resulting difference in energy between island growth and layer growth is given by Eq. (5) and illustrated in Figure 9.

$$\Delta W = W_{\text{surf}} + W_{\text{relax}} = const_1 \gamma d^2 - const_2 k \xi^2 d^3 \tag{5}$$

k = bulk modulus, ξ = strain

Considering films of the same volume content, the increased surface energy for the island growth Figure 8b, is proportional to the island area, d^2 , whereas the energy released by relaxation of the lattice is proportional to the island volume, d^3. A relaxation

mode which is characteristic of isolated islands is shown in Figure 10 for a case where the film material has a larger bulk lattice parameter than the substrate. The model predicts a critical value, d_{crit}, where the island growth is finally more favourable and a fast decrease of the energy for larger sizes. However, the limits of the model are reached in this region as the simple relaxation mode is obviously no longer valid for large sizes.

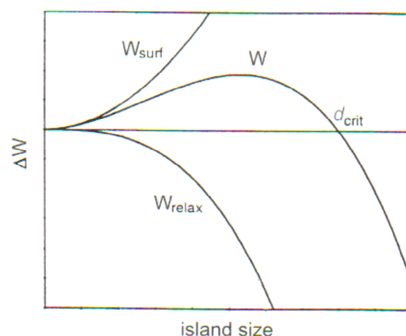

Figure 9: Energy contributions as a function of the island size [5].

2.4 Strain Relaxation in Continuous Films

Along with film growth, the islands will overlap and a closed film will form, which can no longer relax by the mechanism discussed above. A possible mechanism for strain relaxation is the formation of **misfit dislocations** as schematically shown in Figure 11. As long as the film is rather thin, there is perfect epitaxy on the substrate, however, the unit cell is tetragonally distorted; as the in-plane lattice parameter is forced to smaller values, an expansion, according to Poisson's ratio, is observed in the direction perpendicular to the film. This tetragonal structure is manifested by the different in-plane and out-of-plane lattice parameters and by a tilt of the crystallographic angles, e.g., a deviation of the [110] direction from 45 °. This strain is relaxed by the formation of dislocations as indicated in Figure 11b, and the film returns, in principle, to the cubic structure, however, the interface is only semi-coherent.

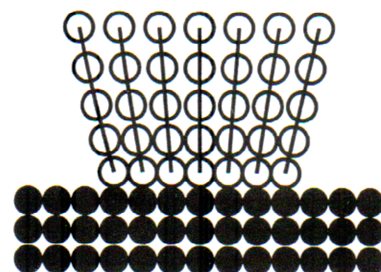

Figure 10: Strain relaxation in pseudo-morphic (dislocation - free) islands.

3 Physical Deposition Methods

In this Section, we will give a short introduction to the basic principles of the different physical deposition methods and some comments on their advantages and drawbacks. Some special features of the different techniques will be demonstrated by examples which are selected to additionally demonstrate the wide field of thin-film applications in microelectronics and the wide spectrum of analytical tools for the characterization of thin films.

3.1 Thermal Evaporation / Molecular Beam Epitaxy

Molecular beam epitaxy (MBE) has evolved from simple thermal evaporation techniques by the application of UHV techniques to avoid disturbances by residual gases, and additionally includes many different sources. A schematic view of a system is shown in Figure 12 including several different sources which allow the controlled deposition of multi-element compounds. The main components and their use are summarized in Table 3: these are the different beam sources, the shutters, which are very important for controlling the growth of dopant profiles or multi-layers, the process environment and, very specific for MBE, the in-situ process control. Due to the UHV environment all UHV surface techniques might be applied, but only reflection high energy electron diffraction (RHEED) is included here as an example.

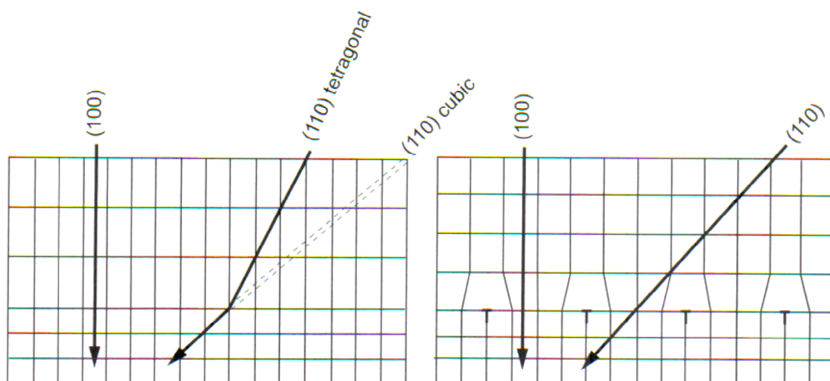

Figure 11: Strain relaxation by misfit dislocations for the example of two initially cubic crystals. As the film has a larger lattice constant than the substrate the forced matching at the interface yields a tetragonal distortion of the film. By misfit dislocations this strain can be relaxed and the film can re-approach its cubic structure.

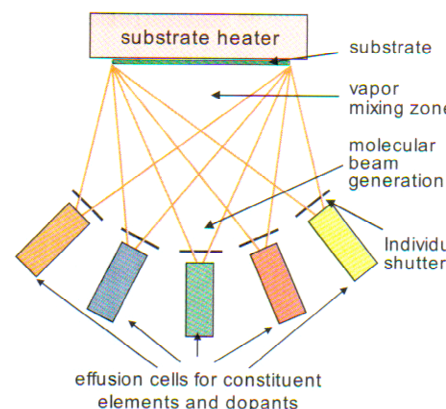

Figure 12: Schematic view of a MBE system for the growth of multi-element compound films.

Facilities	Components	Functions
Beam generators	Knudsen cells e^-- beam evaporators Gas or vapour cells	To provide stable, high-purity, atomic or molecular beams impinging onto substrate surface ⇒ MOMBE
Beam interruptors	Fast-action shutters	To completely close or open line of sight between source and substrate. Action should be rapid (< 0.1 s) and should cause minimal thermal disruption of source
Process environment	Multichamber UHV system	To provide ultraclean growth environment, with residual gas species (e.g. O_2,CO, H_2O,CO_2) < 10^{-11} mbar
Beam and growth monitors	RHEED Beam monitoring ionization gauge mass spectrometer	To provide dynamic information on the surface structure on beam intensities and on compositional information

Table 3: Principle operative systems in MBE and their function (after Parker [6]).

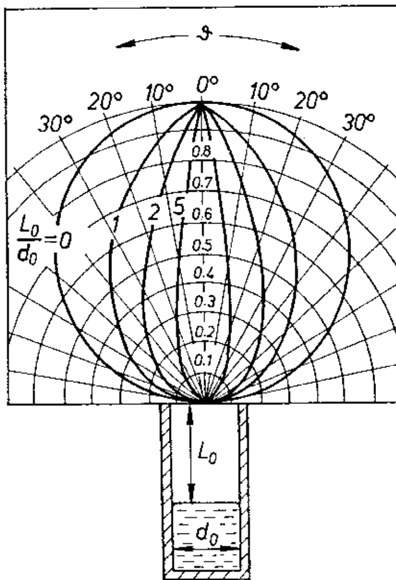

Figure 13: Schematics of a Knudsen cell and the distribution of the vapour beam intensity [7]. The distribution depends on the ratio L_0/d_0 and consequently on the filling level of the cell.

3.1.1 Sources

The schematic of the classical MBE source, the Knudsen cell, is illustrated in Figure 13. The evaporation rate, N_c, is described by the Hertz-Knudsen (or Langmuir) equation:

$$N_c = \frac{p_c A_c}{\sqrt{2\pi m k_B T}} \quad (6)$$

p_c is the equilibrium vapour pressure and A_e the area of the aperture [7]. Therefore, the source can be precisely controlled by a single parameter, the temperature. However, the technical details are very complex and involve more parameters than shown in Eq. (6) .

Figure 14 shows the principle of an electron beam evaporator. The electron beam is magnetically deflected by 270° and is centred on the source material. In this way a melt of the source material is produced on a block of the same material which can be held in a water-cooled cold crucible in order to avoid contamination of the melt.

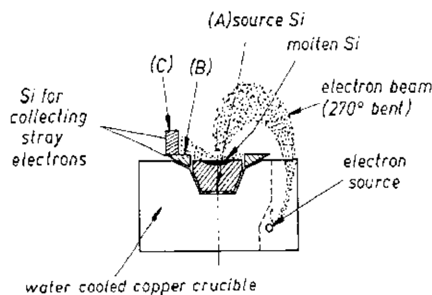

Figure 14: Schematics of a electron beam evaporator for Si evaporation [7]; B: Si guard ring, C: catcher for backscattered electrons.

3.1.2 Process Environment

Larger MBE systems are composed of modular stainless steel building blocks and Figure 15 gives an example: the deposition chamber, the wafer or substrate preparation chamber and often an additional analytical chamber. All operative components are attached by flanges for service access. All materials used within the system need special consideration in terms of low gas desorption and high resistance to heating during out-gasing at elevated temperatures. Parts with high heat load are liquid-nitrogen-cooled ('cryo panel') . Pumping systems include turbomolecular pumps, especially in parts with larger gas load, cryopumps and ion getter pumps.

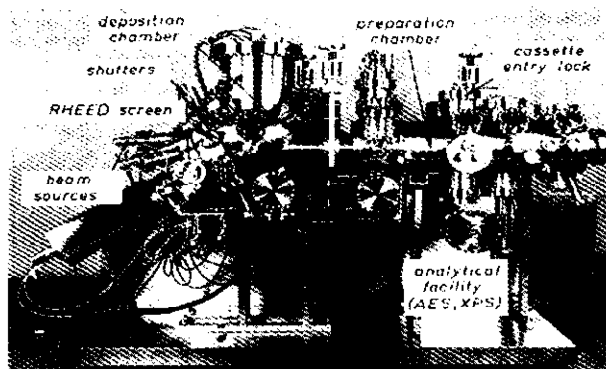

Figure 15: Overview of an MBE system [7].

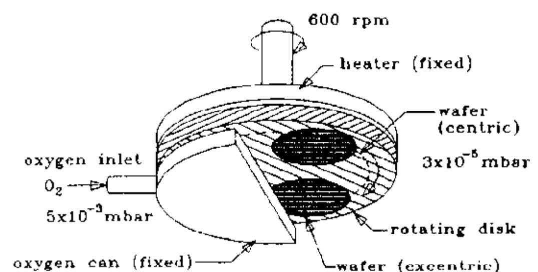

Figure 16: Control of the oxygen partial pressure by differential pumping [8].